Colloidal stability study of Fe_3O_4-based nanofluids in water and ethylene glycol

Caio C. dos Santos[1] · W. R. Viali[1,2] · E. S. N. Viali[2] · R. F. C. Marques[1] · M. Jafelicci Junior[1]

Abstract

In this work, we report the synthesis of a new nanofluid (NF) based on magnetic nanoparticles (MNPS) synthesized by the coprecipitation method with high colloidal stability. The MNPS were functionalized with citric acid (Cac), and then, polyethylene glycol, 1000 (PEG1000), was bonded by polycondensation reactions with acid groups on the nanoparticles surface to increase the colloidal stability of the nanofluid. The MNPS were dispersed in an aqueous medium to obtain nanofluid-based magnetic nanoparticles in water (NF-MNPS-W) and in ethylene glycol to obtain nanofluid-based magnetic nanoparticles in ethylene glycol (NF-MNPS-E). The MNPS were characterized by X-ray diffraction and selected area electron diffraction, which confirmed the formation of the crystalline phase of Fe_3O_4. Transmission electron microscopy was used to confirm the size and morphology of the MNPS. The MNPS had an average diameter of 11.33 ± 3.68 nm. Infrared spectrum of the MNPS allowed the functionalization of the MNPS by Cac and then by PEG1000 to be proved. The colloidal stability of NF-MNPS-W (pH 8) and NF-MNPS-E was evaluated by measurement of Zeta potential (ζ) and dynamic light scattering (DLS) -25 mV and 112 nm ± 1 nm, respectively. The DLS in the temperature function allowed the stability of the NF to be proved in working conditions.

Abbreviations

Cac	Citric acid
Dh	Hydrodynamic diameter
DLS	Dynamic light scattering
D_{TEM}	Diameter size
FTIR	Fourier transform infrared spectrum
IEP	Isoelectric point
MNPS	Magnetic nanoparticles
MNPS-Cac	Magnetic nanoparticles surface modified with citric acid
MNPS-Cac-PEG1000	Magnetic nanoparticles surface modified with citric acid and PEG1000
NF	Nanofluid
NF-MNPS-E	Nanofluid-based magnetic nanoparticles in ethylene glycol
NF-MNPS-W	Nanofluid-based magnetic nanoparticles in water
NPS	Nanoparticles
PDI	Polydispersity index
PDI_{DLS}	Polydispersity index DLS
PDI_{TEM}	Polydispersity index TEM
PEG1000	Polyethylene glycol 1000
SAED	Selected area electron diffraction
TEM	Transmission electron microscopy
XRD	X-ray diffraction
ζ	Zeta potential

✉ Caio C. dos Santos
caio.cvs@hotmail.com; caio.c.santos@unesp.br

1   Laboratory of Magnetic Materials and Colloids, Department of Physical Chemistry, Institute of Chemistry, São Paulo State University (UNESP), Araraquara, SP, Brazil

2   Goiano Federal Institute of Education, Science, and Technology, Rodovia Sul Goiana Km 01, Zona Rural, Rio Verde, GO Zip code 75.901-970, Brazil

Introduction

The combination of electronic components and the miniaturization of devices are responsible for the production of large amounts of heat flow. Although there has been a growth in the electronics industry, semiconductor technology still presents significant challenges related to refrigeration, which may result in lower performance and lower longevity of the devices. A combination of different cooling techniques has been used to meet the current energy demands [1–7].

As is generally known, high-efficiency electronic devices produce large amounts of heat in small areas, and traditional methods of refrigeration, the use of conventional refrigerants is not able to meet the demand for cooling [8–10]. To overcome research into new materials with more efficient refrigeration capacity has become increasingly intense [11].

In this context, the use of nanofluids (NF), which consist of a colloidal dispersion of highly stable nanoparticles in a traditional refrigerant, has been promising because it has a heat exchange capacity superior to the conventional fluids used in refrigeration [6, 12–15]. Since its conception in the early 1990s, this new class of materials has been considered promising as more efficient heat exchangers. They can be applied as refrigerants in the most diverse areas [16], such as solar collectors [17, 18], vehicles, and refrigeration [19], different means of transportation [9], aerospace [20], cutting and tempering of metals [21], and electronic devices [6, 22].

Besides, their superior cooling capacity can also be combined with microchannel systems and thus considerably increase the efficiency in heat dissipation from electronic devices [19, 22, 23]. More than 20 years of research have been invested since the first report on the superior properties of heat exchange related to the use of NF as refrigerants [24–26]. More recently, articles have been concerned with demonstrating the colloidal stability of these systems, which is critical if NF for use in real systems [27–32].

Researchers have been engaged in the production of NF with appreciable colloidal stability and the study of the colloidal properties of these systems. However, a systematic review is essential, demonstrating colloidal stability over time and presenting the conditions used during this interval (e.g., in steady state or under agitation, at what temperature or in light). Images or data that prove the stability of these NF also needed. It is vital to show the values of the dynamic light scattering (DLS) of the sample, the size distribution curve, and the polydispersity index (PDI) of the sample, factors that prove the quality of the data obtained.

Different NF has been reported in the literature over the past decades [33–36], and the vast majority consisting of nanoparticles (NPS) oxides [37] dispersed in various fluids such as water, ethylene glycol, and refrigerant oils. Oxide NPS have been noted for their ease in obtaining, handling, and cost when compared, for example, to the use of metallic NPS or carbon derivatives. Among oxide NPS, colloidal magnetic nanoparticles (MNPS) dispersions were intensively studied decades before the development of this class of materials now known as NF (previously reported in the literature as ferrofluids or in high concentrations as rheological magnetic fluids) [38–40].

MNPS have unique characteristics that can, for example, allow flow control in microfluidic circuits. Furthermore, these materials are prevalent in the use of drug release [41–43]. MNPS can flow along a magnetic field gradient, which may be useful for the development of micropumps without moving parts that can be a pumping alternative to microsystems [44, 45].

Although the use of MNPS are widespread in the literature and there are many different protocols for obtaining these materials, ensuring the chemical and colloidal stability of this system for an extended period without agglomeration or aggregation occurring is an extremely important factor [46]. After obtaining the MNPS, they are usually able to present colloidal stability at acidic/basic pH regions. This is colloidal stability acquired is due to the loading of the surface of the MNPS at these pH intervals giving electrostatic stability to the colloid [47].

Electrostatic stability is widely reported in the literature, and this system can be well described by DLVO theory [48], but when it comes to nanofluid applications, it is not the best strategy to be used for colloidal stabilization of the system. Electrostatic stability promotes colloidal stability through kinetic mechanisms and, for these to be more efficient, they must be composed of diluted colloidal dispersions. Furthermore, methods based on electrostatic repulsion may be agglomerated/aggregated due to compression in the electric double layer when the system undergoes variations in its ionic strength [49].

Thus, to promote better system stability, the use of the steric stabilization strategy or electrosteric stabilization is the best strategies for colloidal stability in nanomaterials. The first is capable of promoting colloidal stability for the system by creating a physical barrier that prevents two particles from getting close, decreasing the entropy of the system in addition to having an increase in the osmotic gradient caused when particles approach one another, factors that significantly increase the colloidal stability of the system compared to electrostatic stability [49]. The third (electrosteric) strategy that can be adopted comes from the combination of the mentioned strategies promoting better colloidal stability to the system. Therefore, in this work we produced MNPS, which were coated with citric acid and then functionalized with
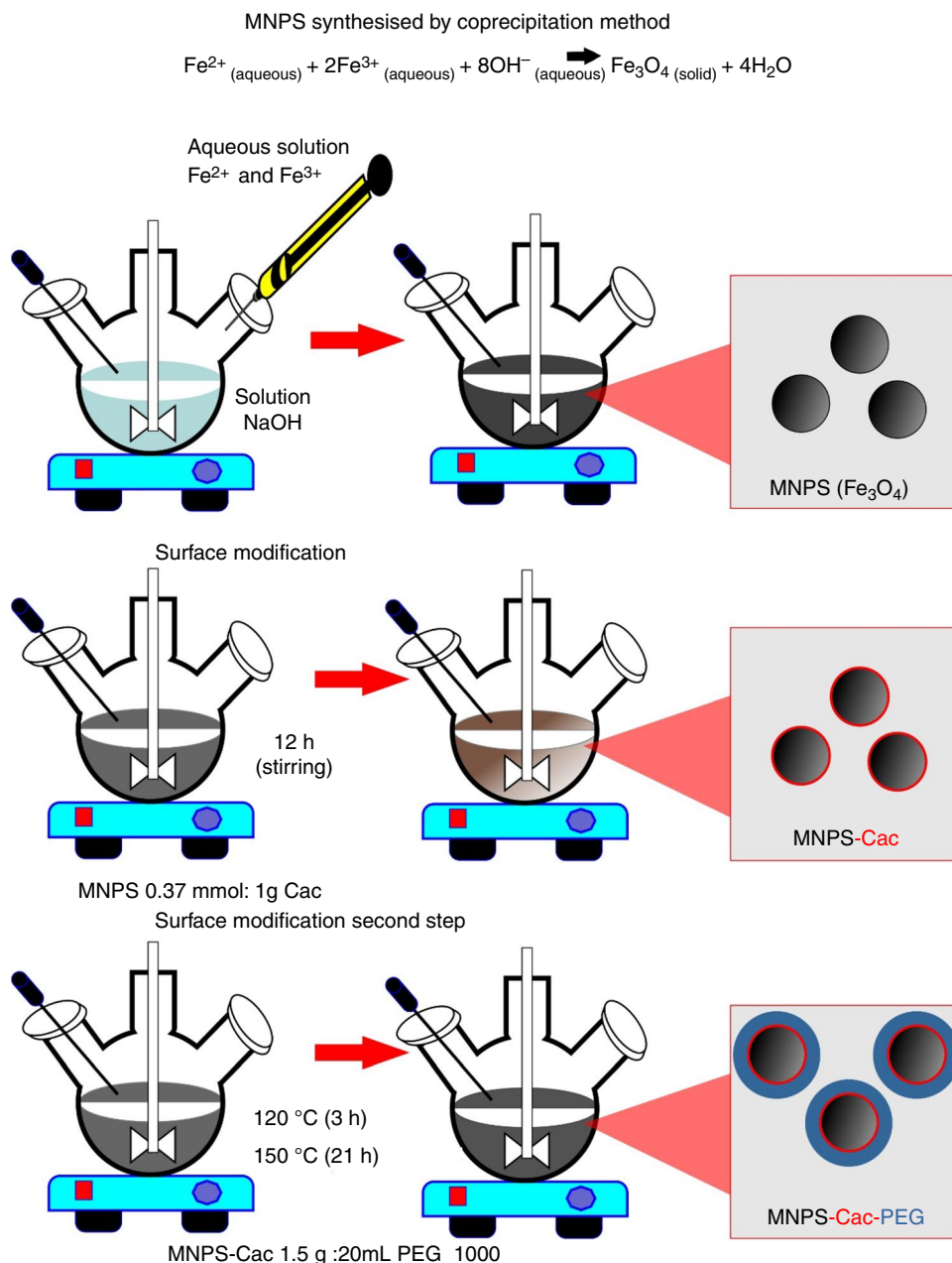
PEG1000, combining the electrostatic and steric stabilization mechanisms, to obtain efficient colloidal stability in the various application conditions, such as dilution and temperature variation.

In this paper, we report the synthesis of two NF (water and ethylene glycol-based), obtained by dispersion of MNPS coated by Cac-PEG1000 and the evaluation of their colloidal stability as a function of the time, heating cycles and, for the water-based fluid, the effect of pH as well.

Materials and methods

All the chemical reagents used in this work presented analytical grade and were used without any purification. For the synthesis, iron(II) chloride tetrahydrate (98%), iron(III) chloride hexahydrate (97%), citric acid (99%), polyethylene glycol 1000, and triglyme (99%) were purchased from Sigma-Aldrich Brazil. Sodium hydroxide (97%) Vetec, sodium chloride (99%), and ethylene glycol were acquired from Neon, and absolute ethanol (99%) was obtained from Synth. Acetone (99%) and hydrochloric acid (38%) were bought from J.T. Baker.

Fig. 1 Synthesis and functionalization of MNPS step by step

MNPS synthesised by coprecipitation method

$$Fe^{2+}_{(aqueous)} + 2Fe^{3+}_{(aqueous)} + 8OH^-_{(aqueous)} \rightarrow Fe_3O_4\ _{(solid)} + 4H_2O$$

Aqueous solution Fe^{2+} and Fe^{3+}

Solution NaOH

MNPS (Fe$_3$O$_4$)

Surface modification

12 h (stirring)

MNPS 0.37 mmol: 1g Cac

MNPS-Cac

Surface modification second step

120 °C (3 h)
150 °C (21 h)

MNPS-Cac 1.5 g :20mL PEG 1000
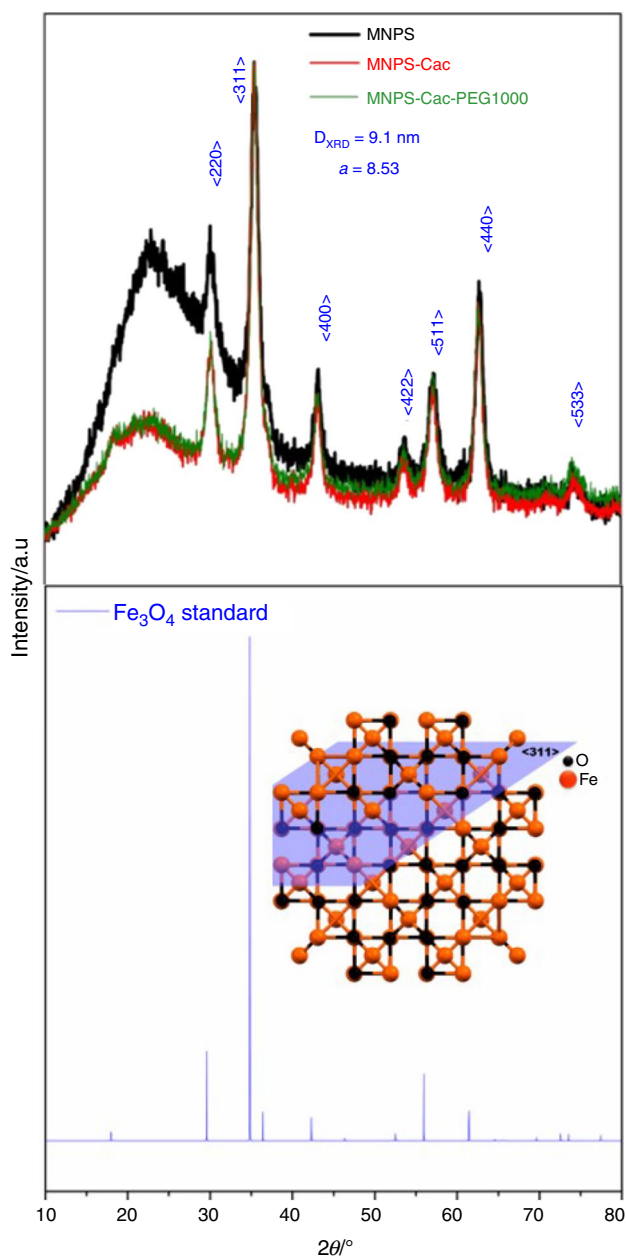
MNPS-Cac-PEG

Fig. 2 X-ray standard diffraction of the MNPS (black), MNPS-Cac (red), and MNPS-Cac-PEG1000 (green) and standard magnetite (pdf JPCDS 79-419). (Color figure online)

Experimental

The MNPS were synthesized by coprecipitation of the mixture of iron(II), and iron(III) ions in alkaline medium with modifications [12] Fig. 1 shows the scheme used for the synthesis and functionalization step by step. Briefly, a solution containing 0.04 mol of $FeCl_2$, and 0.08 mol of $FeCl_3$ was dropped into hydroxide solution 1.5 mol L^{-1}

under mechanical stirring and inert atmosphere. The solution was stirred for 12 h at 100 °C. The MNPS produced were washed with distilled water until pH 9.0. After that, the MNPS were functionalized [50] with citric acid (Cac), magnetic nanoparticles were surface modified with citric acid (MNPS-Cac), and 0.37 mmol of Cac was added for each 1 g of MNPS and kept under stirring overnight. The MNPS-Cac produced were washed with distilled water and ethanol. In the peglaytion step, polyethylene glycol, 1000 (PEG1000), was bonded by polycondensation with the citric acid on the surface of the nanoparticles to produce the surface of the magnetic nanoparticles modified with citric acid and PEG1000 (MNPS-Cac-PEG1000). Then, 1.5 g of wet MNPS-Cac was dispersed in triglyme, and to it was added 20 mL of PEG1000; this solution was kept in a magnetic stirrer at 120 °C for 3 h under an Argon flow, and then, the temperature was raised to 150 °C for 21 h. The MNPS-Cac-PEG1000 produced were washed three times with acetone [50]. Finally, this material was divided into two parts, one added to 50 mL water and the other one added to 50 mL ethylene glycol, to produce the NF-MNPS-W and NF-MNPS-E. The dispersions were carried out by stirring overturning, and after adding the desired mass (1.15 g) to the solvent (50 mL), the nanomaterials stayed under stirring for 24 h at 10 rpm.

The X-ray diffractogram was obtained in a model 5005 with CuKα radiation (I = 1.5418 Å) with a 40 kV and 40 mA, in the range of 20 to 80 degrees. The infrared spectra (FTIR) of the sample were performed using a Frontier FTIR spectrometer from PerkinElmer using diffuse absorption spectroscopy. The analysis was measured using 64 scans for accumulation data and 4 cm^{-1} of resolution in 4000 at 400 cm^{-1} range. The micrograph of MNPS has performed in a transmission electron microscope Philips CM120 microscope at 120 kV. The TGA curves were obtained in the TGA 4000 thermoanalyzer, from PerkinElmer. The analyses were performed under the following conditions: temperature range from 35 to 900 °C, the heating ratio of 10 °C min^{-1}, under dry air with a flow rate of 10 mL min^{-1} in an α-alumina crucible. The determination of the degree of covering was carried out, considering the average diameter of the MNPS obtained by TEM, for the calculation of the number of particles present in 1 g and the surface area of a MNPS, with the TGA data the mass was related to loss of organic matter in the samples, and the approximate amount of coating molecules present in this mass was calculated, from the ratio between the number of molecules and the surface area of a nanoparticle, the degree of coating of the number of molecules per nm^2 of the MNPS surface. The colloidal stability was evaluated by the analyses of the zeta potential (ζ) and DLS using a Zetasizer Nano series ZS equipment from Malvern Instruments. Measurements
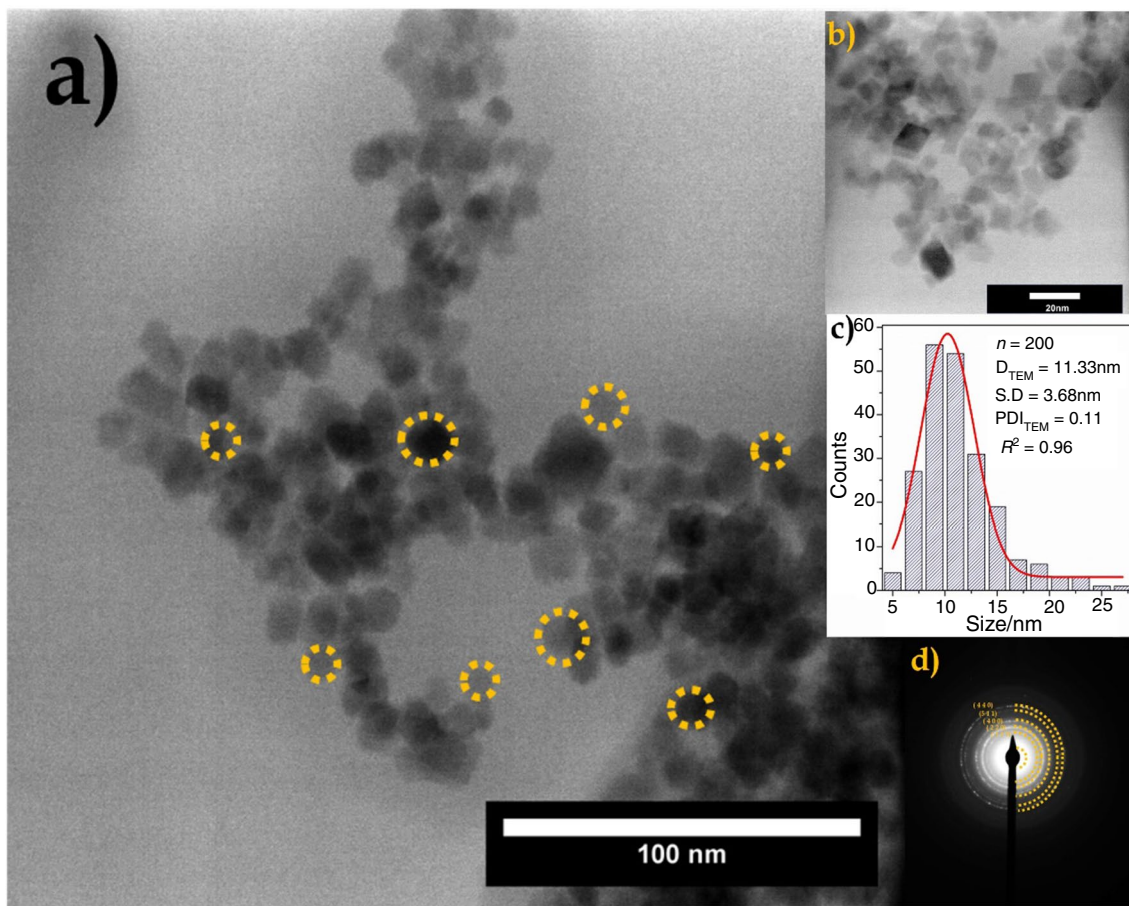
Fig. 3 Micrograph of sample **a** and **b** image transmission electron microscopy (TEM) and **c** histogram counts of the MNPS and **d** shown the selected area electron diffraction (SAED) of MNPS
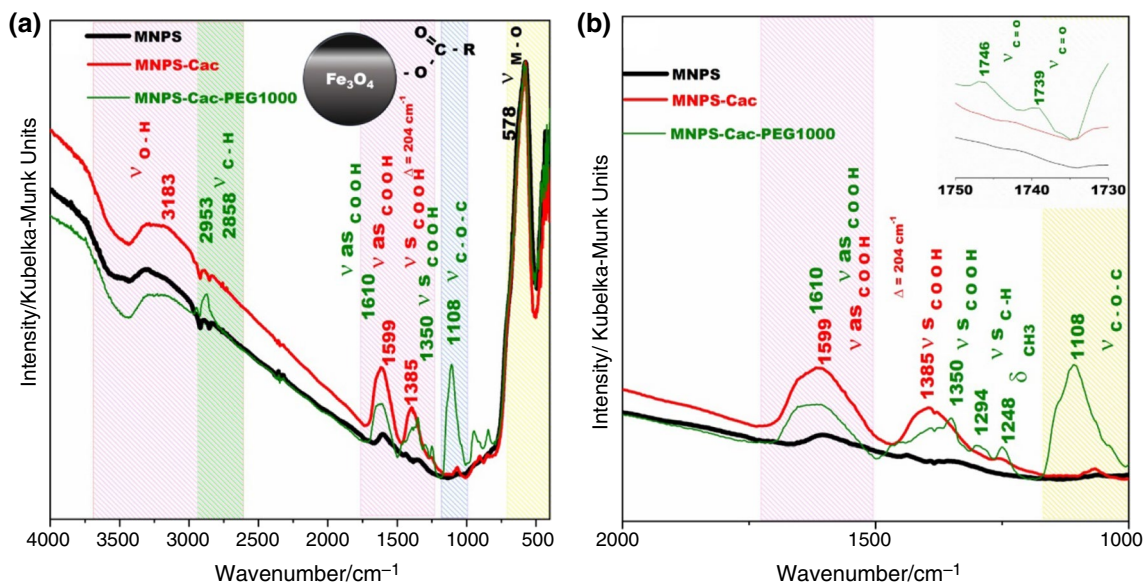

Fig. 4 **a** FTIR spectra of the MNPS, MNPS-Cac, and MNPS-Cac-PEG1000 in the range 4000 to 400 cm⁻¹ (Left) and **b** magnification on region 2000 to 1000 cm⁻¹ the inset shows the ester bands region (right)
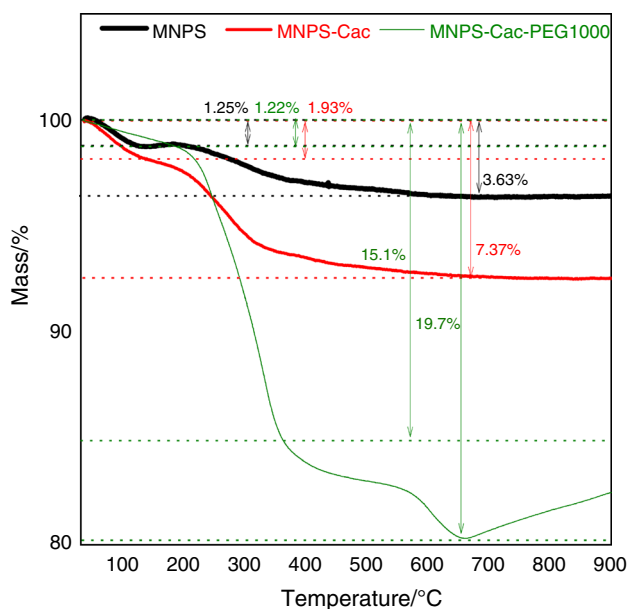
Fig. 5 TGA curves of the samples MNPS, MNPS-Cac, and MNPS-Cac-PEG1000

of DLS as a function of temperature were taken from the dilution of the NF samples in ultrapure water or ethylene glycol. For the measurements as a function of temperature, the samples were added to a glass cuvette, and the analyses were performed using 600 s for temperature equilibrium and performed in triplicate. After the analyses, the samples were discarded. The hydrodynamic diameter average was performed by cumulative analysis, and the final value obtained was the average of the Z-average triplicate, and all data presented are related to the intensity of scattered light. The Zeta potential was measured by dispersing 50 microliters of NF in 1 mL of solution (water, sodium chloride 1 and 10 mmol L^{-1}). Then, the samples were titrated in the pH range 3 to 10 with an interval of pH units measured in triplicate with 30 s between each measurement, using hydrochloric acid (HCl, 0.1 mol L^{-1}) and sodium hydroxide (NaOH, 0.1 mol L^{-1}) as titrants.

Discussion and results

The crystallographic structure of the MNPS was evaluated by the XRD analyses. Figure 2 shows the XRD patterns of the MNPS.

As observed, the sample showed characteristic reflection patterns according to the crystalline structure standard of magnetite (pdf JPCDS 79-419). The lattice parameter was $a = 8.530$, which is approximately equal to the standard magnetite. The size of the crystallites was calculated based on Scherrer's law, using the width at half-height of the most

intense peak <311> and considering the approximately spherical MNPS, the average size of the crystallites was of 9.1 nm [50, 51]. Figure 3 shows the morphology and the diameter distribution of the MNPS.

As can be observed in Fig. 3a, b, the roughly spherical morphology of the MNPS and the average diameter size (D_{TEM}) obtained by the counts of the images from transmission electron microscopy (TEM), the MNPS had an average diameter of 11.33 ± 3.68 nm Fig. 3c. Figure 3d shows the selected area electron diffraction (SAED), in which indexation of the MNPS is performed by software *Crystbox7* and the crystalline phase of the MNPS is confirmed as magnetite PDF card number 79-419 from the JPCDS database. The size histogram of the MNPS sample was obtained by counts of 200 particles and using a Gaussian distribution function with $R^2 = 0.96$. The calculated polydispersity index (PDI_{TEM}) acquired by the square of the rate of the standard deviation by D_{TEM} is 0.11, and this indicated that the MNPS synthesis is monodisperse (monodisperse materials show PDI_{TEM} close to 0.1) [52].

Figure 4 shows the spectra in the infrared region, confirming the coating of the MNPS in different steps of the surface modification.

The characteristic band is shown in Fig. 4 in the region of 3183 cm^{-1} attributed to the O–H stretch [53]; the bands in the range of 2953 and 2858 cm^{-1} to the C–H stretch [54] and the bands in the region of 578 cm^{-1} were assigned to the M–O stretch [53]. MNPS-Cac presents absorption bands in 1599 and 1385 cm^{-1} that were attributed to asymmetrical and symmetrical COOH stretches and confirm the modification of the surface of the MNPS by Cac [54]. The difference between these bands was calculated as $\Delta = 204$ cm^{-1}, and this gives evidence that the Cac bridges the iron atoms [53].

The other bands confirm the presence of PEG1000 in the sample. As observed, the asymmetrical and symmetrical stretches were shifted to 1610 and 1385 cm^{-1}, respectively, indicating the change in the chemical environment caused by PEG1000 [55, 56]. However, the characteristic band of C=O stretch esters that would confirm the reaction between PEG1000 and Cac is of low intensity, indicating that only a small amount of sample would be bound to PEG1000 (Inset Fig. 4b) [55, 56]. The band in the 1294 cm^{-1} region was assigned to the C–H stretch, and the 1248 cm^{-1} band was attributed to the CH_3 strain. Finally, the original PEG band at 1108 cm^{-1} was attributed to the C–O–C stretch [57, 58].

Figure 5 shows the three TGA curves of the samples (MNPS, MNPS-Cac, and MNPS-Cac-PEG1000). Their specific thermal events are described in detail.

All the TGA curves show the first thermal event attributed (range 30–175 °C) to the desorption of water molecules adsorption at the NPS surface. This event is associated with a small mass loss that was 1.25, 1.93, and 1.22% for the MNPS, MNPS-Cac, and MNPS-Cac-PEG1000 samples,

Fig. 6 Zeta potential as a function of pH of the samples in different medium (water, NaCl 0,01, and NaCl 0,01 mol L^{-1}) **a** MNPS, **b** MNPS-Cac and **c** MNPS-Cac-PEG1000

respectively. For the MNPS sample, only one more slow thermal event is observed associated with hydration water molecules leading to a total mass loss of 3.63% for the MNPS-Cac presented in the thermal event, which can be related to loss of organic matter (7.37%). The MNPS-Cac-PEG1000 showed three more thermal events, the first two associated with loss of organic matter at 361 and 659 °C with mass losses of 15.1 and 19.7%. The last observed thermal event, which starts at 659 °C, is associated with a mass gain caused by the oxidation of magnetite to maghemite. However, the total mass gain cannot be completed in the temperature range analyzed.

Based on the data obtained from the loss of organic matter of the samples and knowing the size of the sample nanoparticle (11.33 nm), as shown in Fig. 5, it was possible to calculate the degree of coating of the samples. For sample MNPS-Cac, the degree of Cac coating was 1.13 Cac molecules per nm^2 surface area of MNPS, indicating that Cac forms something close to a monolayer over MNPS, considering the bonding area of a carboxylate 0.25 nm^2 [50, 59, 60]. For the MNPS-Cac-PEG1000 sample, the coated PEG1000 shows the number of molecules for the particle to be approximately 316, which leads to an estimate that the molecule ratio of Cac/PEG1000 is 1.5 coating the nanoparticles. TGA analyses of the sample at different heating ratios (10, 20, 25, 30 and 35 °C min^{-1}) allowed the calculation of the activation energy required for the loss of approximately 10% of the sample mass according to ASTM E1641. The activation energy in this process was about 109.6 kJ mol^{-1}, which indicated the thermal stability promoted by coating the sample.

The colloidal stability of the NF was evaluated by measurements of the zeta potential as a function of pH shown in Fig. 6.

The isoelectric point (IEP), the MNPS, MNPS-Cac and MNPS-CacPEG1000 were at pH 6.7, 3.1, and 3.6, respectively. In Figure 6a, Zeta potential curves present the characteristic profile of the MNPS curve as a function of pH. Zeta potential above the minimum limit (25 MV in modulus) [61] is needed for electrostatic system stability at pH values below 4 and above 8. This is characterized by the formation on the surface of Fe–OH₂$^+$ species in acidic regions and Fe–O$^-$ species in alkaline regions [62]. After the first functionalization stage, Cac modifies the surface of MNPS by oxygen binding of Cac carboxylate. In the literature, Cac presents pKa at 4.2 [40, 63]; therefore, below pH 4, there is a predominance of the protonated form of this acid, whereas, at a higher pH, the acid is found in its deprotonated form, which confers a negative potential observed for this acid in
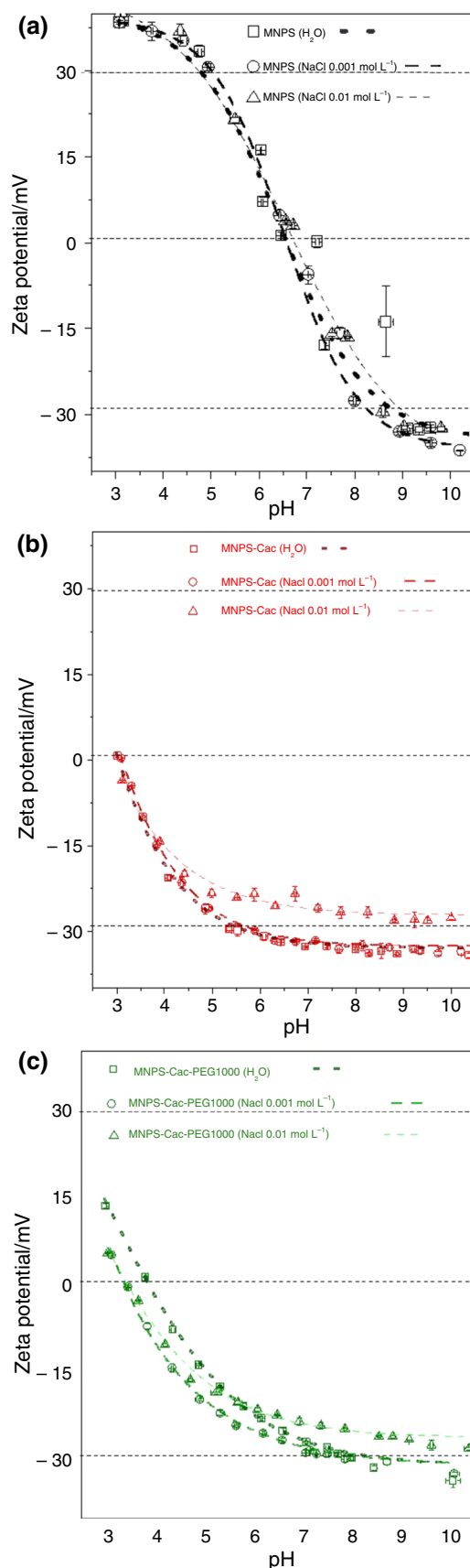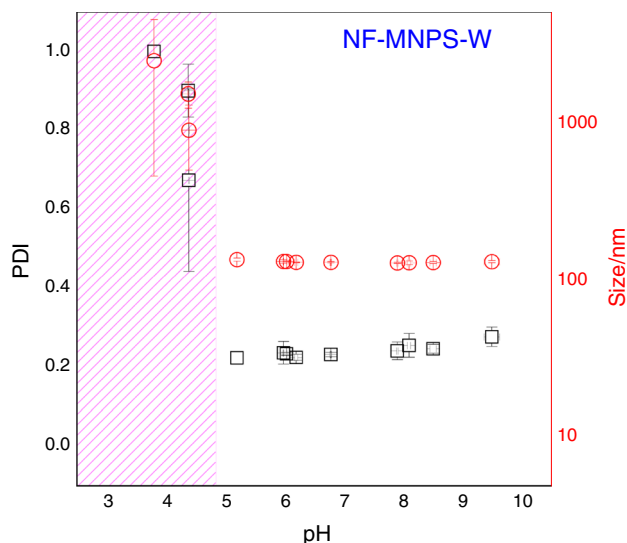
Fig. 7 Hydrodynamic diameter size (red) and polydispersity index (PDI$_{DLS}$) (in black) as a function of pH of the samples MNPS-Cac-PEG1000 (NF-MNPS-W). (Color figure online)

the sample MNPS-Cac. After the functionalization step, the PEG1000 saw a decrease (in modulus) of the potential due to the interaction between some Cac functional groups and the PEG1000 molecules. This diminished the contributions of the electrostatic stability to the system but contributed to the steric stability. In this way, a system with electrosteric colloidal stability is formed. Above pH 5.5, the sample shows a value of the zeta potential in modulus (25 mV), which gives the minimum electrostatic stability. Therefore, the final pH of the aqueous NF was adjusted to 8.0. The attachment of

PEG onto the MNPS surface added higher dispersibility and colloidal stability in aqueous media compared with citrate-coated [50]. The addition of NaCl electrolyte at a higher concentration (0.01 mol L^{-1}) decreases the zeta potential magnitude, due to the effect known as "double electric layer compression." The ionic strength increases in the system, caused by the addition of the electrolyte, and therefore leads to a decrease in the magnitude of the zeta potential and the electrostatic stability of the colloidal dispersions [32, 50, 64]. Figure 7 evaluated the colloidal stability of the aqueous nanofluid NF-MNPS-W in the function of the pH.

The DLS data in Fig. 7 corroborate what is observed in the zeta potential curve for the MNPS-Cac sample. Above pH 5, the sample has appreciable electrostatic stability where no significant changes in the hydrodynamic diameter and polydispersity index values of the sample are observed. For lower pH values, however, the electrostatic stability is smaller, and a rapid increase in hydrodynamic diameter and polydispersity index values is observed, indicating the agglomeration/aggregation of the system particles. (The size distribution curves as a function of pH were added as support material Fig.Sup.01.)

Figure 8 shows the data of the zeta potential variation as a function of sample temperature NF-MNPS-W in different values of pH. In Fig. 8a, the behavior of the zeta potential of the NF-MNPS-W pH8 sample is shown when subjected to temperature variations. As expected with increasing temperature, the magnitude of the zeta potential decreases since with increasing temperature, there is a decrease in the viscosity of the medium that is directly proportional to the zeta potential [59, 65, 66]. Although there is a slight decrease in the magnitude of the zeta potential, the sample in this temperature range showed
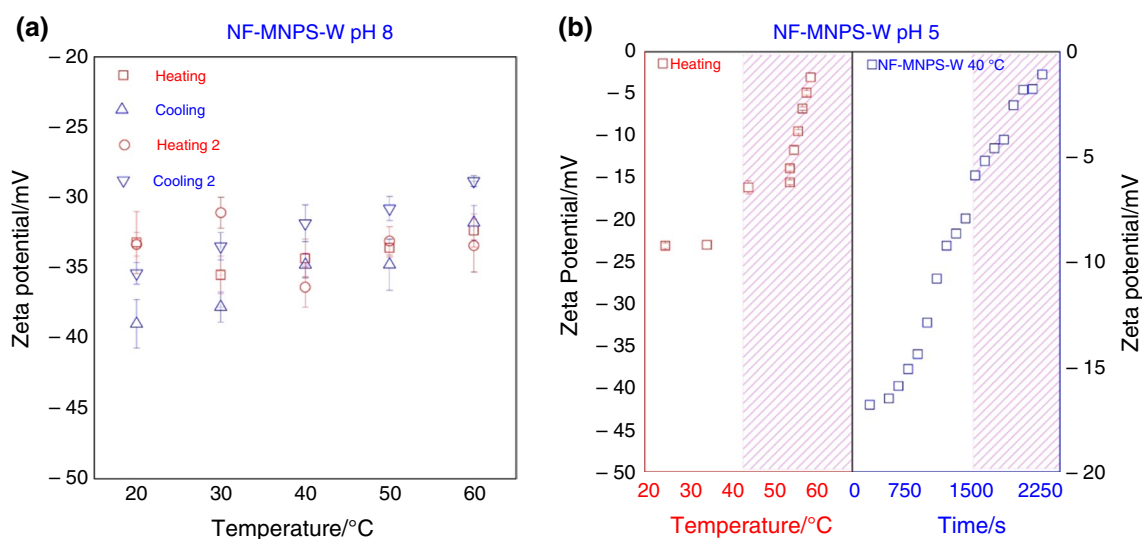

Fig. 8 **a** Zeta potential in the function of the temperature of the sample NF-MNPS-W pH eight and **b** zeta potential in the function of the temperature of the sample NF-MNPS-W pH five and in the function of the time at 40 °C
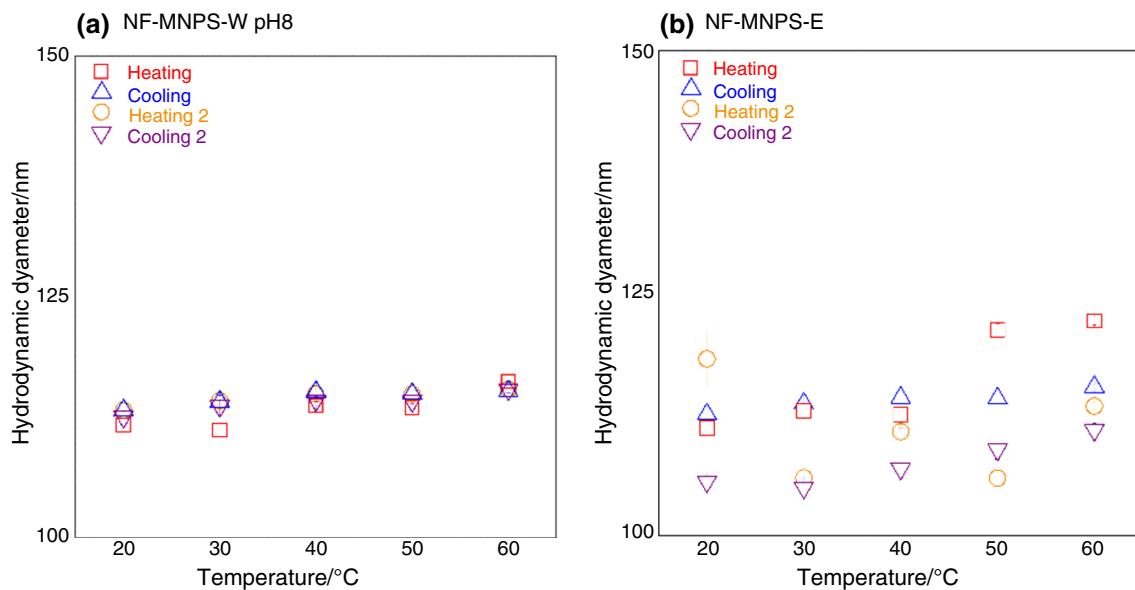
Fig. 9 Colloidal stability of the samples evaluated by DLS in the function of the temperature **a** hydrodynamic diameter size in function of the temperature of the sample NF-MNPS-W (left) and **b** hydrodynamic diameter size in function of the temperature of the sample NF-MNPS-E (right)

colloidal stability even after repeated heating and cooling cycles of the sample. In Fig. 8b, the importance of zeta potential value above 25 mV (in modulus) to nanofluid stability is observed, because the temperature influence is critical, and this will promote the quick agglomeration of nanomaterial the under this limit when the temperature of the fluid is increased. For NF-MNPS-W pH5, the sample has a zeta potential value lower than the electrostatic stability limit. Thus, the heating of the sample becomes more significant in the destabilization of the NF, as can be observed from 40 °C, and despite the polymer coating, the sample is subject to destabilization. The magnitude of the zeta potential decreases to near the isoelectric point of the sample. This decrease leads to loss of colloidal stability and phase separation. In Fig. 8c, the temperature of NF-MNPS-W pH5 was set at 40 °C and the variation in zeta potential as a function of time was observed; the sample gradually loses colloidal stability, and after 2250 s there is a change in behavior due to agglomeration of the sample.

To assess the stability of nanofluids under real working conditions, NF-MNPS-W pH8 and NF-MNPS-E DLS measurements were performed as a function of temperature, as shown in Fig. 9.

As noted, the Dh of the two NF does not change significantly with the heating and cooling of the sample, because nanomaterial agglomeration caused by changes in system temperature is not observed, which is due to the use of electrosteric stabilization of Cac-PEG1000 functionalized nanoparticles, providing a higher stabilization capacity than commonly

used electrostatic stabilization. While electrostatic stabilization is susceptible to temperature variations that can cause nanomaterials to agglomerate because it is a kinetic stabilization, electrosteric stabilization has the alternative to increase the colloidal stability of the system through contributions of steric stability, which can add to the system promoting thermodynamic stability to nanomaterials. These results are displayed in Fig. 9, which characterizes the colloidal stability of the NF against the working conditions of refrigerant fluid.

The colloidal stability of nanofluids as a function of time was assessed by DLS, as shown in Fig. 10. Figure 10 evaluates the colloidal stability of the nanofluids: Fig. 10a–c show the initial DLS results for samples NF-MNPS-W pH5, NF-MNPS-W pH8, and NF-MNPS-E, respectively. The samples were stored and were stirred with overturning at low revolutions per minute, and in Fig. 10d–f, the results of DLS are presented after 160 days. As observed by the DLS data presented and by the photographs in the insets presented in Fig. 10c initial and Fig. 10f after 160 days, in these conditions, the only sample that showed to be unstable and separated phases was NF-MNPS-W pH5, but it was necessary to re-disperse the sample again for the analysis shown in Fig. 10c through the ultrasound bath. Although in the other samples the separation of phases was not observed, increases in the hydrodynamic diameter of the samples can be observed and the aging of the sample may indicate a destabilization of the sample due to the function of long
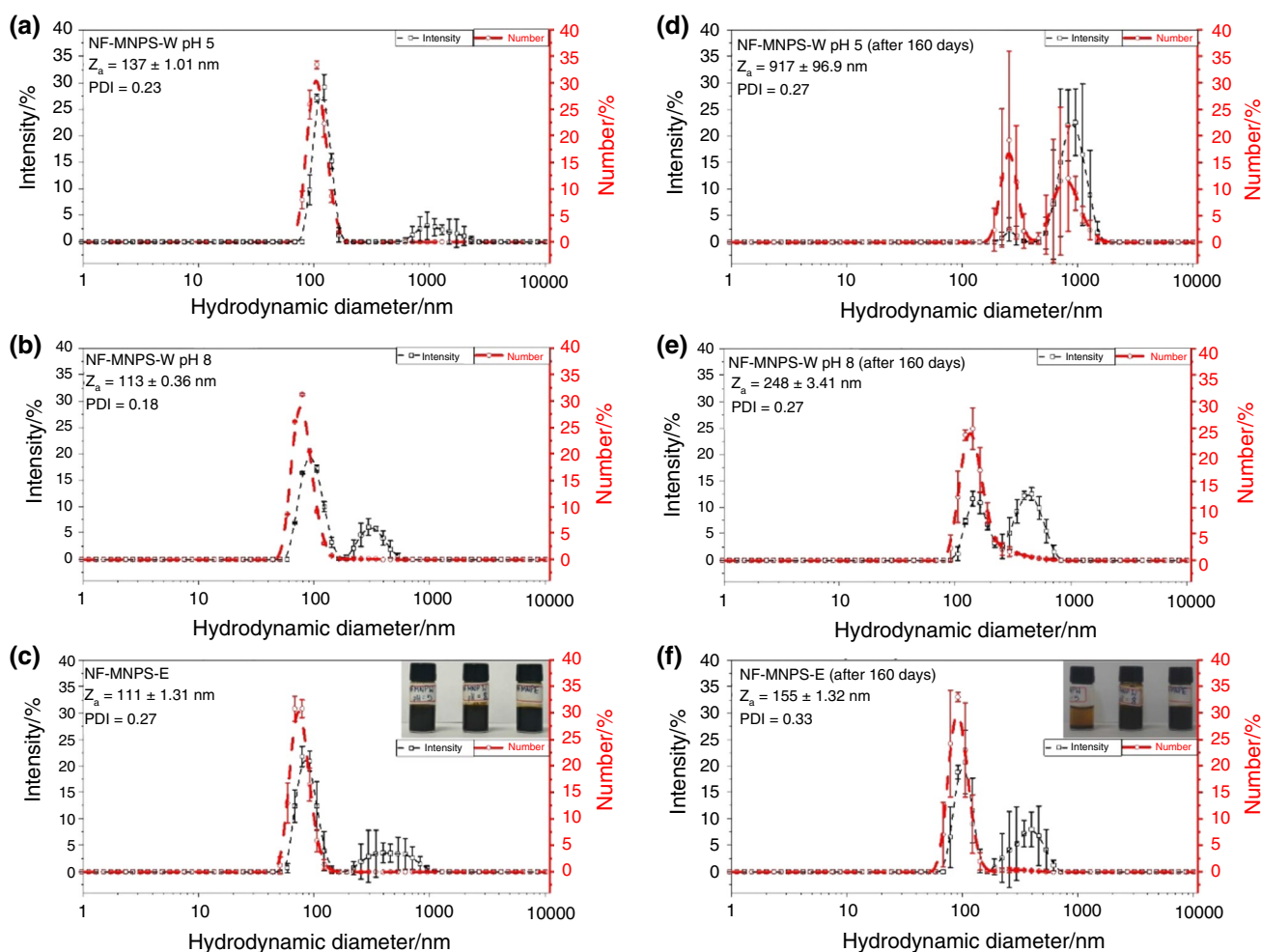
Fig. 10 Colloidal stability of the samples evaluated by DLS **a** first DLS of NF-MNPS-W pH5, **b** first DLS of NF-MNPS-W pH8, **c** first DLS of NF-MNPS-E, on inset shows the samples in initial time, **d** DLS after 160 days for the sample NF-MNPS-pH5, in stirring over- turning (the NF-MNPS-W-pH5 was redispersion), **e** DLS after 160 days for the sample NF-MNPS-pH8, stirring overturning, and **f** DLS after 160 days for the sample NF-MNPS-E, stirring overturning, on the inset shows the image of the samples after 160 days

periods, observed by the increased contribution of families in the agglomerates.

Conclusions

In this work, we used peglaytion methodology to obtain stable NF based on Cac-PEG-functionalized magnetite dispersed in ethylene glycol and water. The pegylation step was adequate to obtain NPS with a coating degree that enables the colloidal stabilization mechanisms in the system. MNPS-Cac-PEG1000 were shown to be easily dispersed in water, and ethylene glycol and the resulting NF exhibited excellent colloidal stability. The Dh, when the nanofluids are subjected to heating and cooling cycles, showed no significant changes in the base fluids used, indi- cating that they can be used as nanofluids. Dh did not change significantly when the sample was submitted to heating and cooling heat cycles to evaluated. This shows that these materials are promising for use as nanofluids.

References

1. Hajatzadeh A, Aghakhani S, Afrand M, Mahmoudi B. An updated review on application of nanofluids in heat exchangers for saving energy. Energy Convers Manag. 2019;198:111886.
2. Mahbubul IM. Application of nanofluid 8.1. In: Preparation, char- acterization, properties, and application of nanofluid. 2019. https://doi.org/10.1016/b978-0-12-813245-6.00008-3.
3. Wahab A, Hassan A, Arslan M, Babar H, Usman M. Solar energy systems—potential of nanofluids. J Mol Liq. 2019;289:111049.

4. Kumar A, Subudhi S. Preparation, characterization and heat transfer analysis of nanofluids used for engine cooling. Appl Therm Eng. 2019;160:114092.

5. Al-rashed MH, Dzido G, Korpy M, Smo J, Wójcik J. Investigation on the CPU nanofluid cooling. Microelectron Reliab. 2016;63:159–65. https://doi.org/10.1016/j.microrel.2016.06.016.

6. Bahiraei M, Heshmatian S. Electronics cooling with nanofluids: a critical review. Energy Convers Manag. 2018;172:438–56.

7. Zhu K, Zhuo C, Yabo W, Hailong L, Xiaojing Z, Carsten F. Estimating the maximum energy-saving potential based on IT load and IT load shifting. Energy. 2017;138:902–9.

8. Wang Y, Wang B, Zhu K, Li H, He W, Liu S, Zhu K. Energy saving potential of using heat pipes for CPU cooling. Appl Therm Eng. 2018;143:630–8. https://doi.org/10.1016/j.applthermaleng.2018.07.132.

9. Sajid MU, Ali HM. Recent advances in application of nanofluids in heat transfer devices: a critical review. Renew Sustain Energy Rev. 2019;103:556–92.

10. Krishna VM, Kumar MS. ScienceDirect Numerical analysis of forced convective heat transfer of nanofluids in microchannel for cooling electronic equipment. Mater Today Proc. 2019;17:295–302.

11. Wong KV, De Leon O. Applications of nanofluids: current and future. Adv Mech Eng. 2010;2:519659.

12. Massart R. Preparation of aqueous magnetic liquids in alkaline and acidic media. IEEE Trans Magn. 1981;17:1980–1.

13. Dolatabadi N, Rahmani R, Rahnejat H, Garner CP. Thermal conductivity and molecular heat transport of nanofluids. RSC Adv. 2019;9:2516–24. https://doi.org/10.1039/c8ra08987f.

14. Maji NC, Chakraborty J. Gram-scale green synthesis of copper nanowire powder for nanofluid applications. ACS Sustain Chem Eng. 2019;7:12376–88.

15. Zhu HT, Zhang CY, Tang YM, Wang JX. Novel synthesis and thermal conductivity of CuO nanofluid. J Phys Chem C. 2007;111:1646–50.

16. Saidur R, Leong KY, Mohammad HA. A review on applications and challenges of nanofluids. Renew Sustain Energy Rev. 2011;15:1646–68.

17. Farhana K, Rahman MM, Ramasamy D, Noor MM, Najafi G, Samykano M, Mahamude ASF. Improvement in the performance of solar collectors with nanofluids—a state-of-the-art review. Nano-Struct Nano-Objects. 2019;18:100276.

18. Sharshir SW, Mostafa ME, Essa FA, Kamal M, Ali A. Applications of nanofluids in solar energy: a review of recent advances. Renew Sustain Energy Rev. 2018;82:3483–502.

19. Azwadi N, Sidik C, Noor M, Mohd W, Mamat R. Recent advancement of nanofluids in engine cooling system. Renew Sustain Energy Rev. 2017;75:137–44.

20. Mahmoodi M, Kandelousi S. Cooling process of liquid propellant rocket by means of kerosene-alumina nanofluid. Propuls Power Res. 2016;5:279–86.

21. Kumar A, Kumar A, Rai A. Effects of Minimum Quantity Lubrication (MQL) in machining processes using conventional and nanofluid based cutting fluids: a comprehensive review. J Clean Prod. 2016;127:1–18.

22. Colangelo G, Favale E, Milanese M, De Risi A, Laforgia D. Cooling of electronic devices: nanofluids contribution. Appl Therm Eng. 2017;127:421–35.

23. Subudhi S, Kumar A. Application of nanofluids for radiator cooling. Encycl Renew Sustain Mater. 2019. https://doi.org/10.1016/b978-0-12-803581-8.11463-8.

24. Bozorg M, Fasano M, Cardellini A, Chiavazzo E, Asinari P. A review on the heat and mass transfer phenomena in nanofuid coolants with special focus on automotive applications. Renew Sustain Energy Rev. 2016;60:1615–33.

25. Wu JM, Zhao J. A review of nanofluid heat transfer and critical heat flux enhancement-Research gap to engineering application. Prog Nucl Energy. 2013;66:13–24.

26. Ghadimi A, Saidur R, Metselaar HSC. A review of nanofluid stability properties and characterization in stationary conditions. Int J Heat Mass Transf. 2011;54:4051–68.

27. Navarrete N, Gimeno-furió A, Forner-escrig J, Juliá JE, Mondragón R. Colloidal stability of molten salt -based nanofluids:dynamic light scattering tests at high temperature conditions. Powder Technol. 2019;352:1–10.

28. Fan Y, Chen Y, Liang X, Xu J, Deng T. Dispersion stability of thermal nanofluids. Prog Natural Sci Mater Int. 2017;27:531–42.

29. Briscoe WH. Current opinion in colloid, interface science depletion forces between particles immersed in nanofluids. Curr Opin Colloid Interface Sci. 2015;20:46–53.

30. Pilkington GA, Briscoe WH. Nanofluids mediating surface forces. Adv Colloid Interface Sci. 2012;182:68–84.

31. Sharma SK, Mital GS. Preparation and evaluation of stable nanofluids for heat transfer application: a review. Exp Therm Fluid Sci. 2016;76:202–12. https://doi.org/10.1016/j.expthermflusci.2016.06.029.

32. dos Santos CC, Viali WR, Viali EdaSN, Assis DR, Amantea BE. Aqueous nanofluids based on copper MPA: synthesis and characterization. Mater Res. 2017;20:104–10.

33. Abreu B, Lamas B. Experimental characterization of convective heat transfer with MWCNT based nanofluids under laminar flow conditions. Heat Mass Transf. 2014. https://doi.org/10.1007/s00231-013-1226-8.

34. Maskeen MM, Zeeshan A, Mehmood OU, Hassan M. Heat transfer enhancement in hydromagnetic alumina—copper/water hybrid nanofluid flow over a stretching cylinder. J Therm Anal Calorim. 2019;138(2):1127–36.

35. Akbari A, Hassan M. Experimental investigation of nanofluid stability on thermal performance and flow regimes in pulsating heat pipe. J Therm Anal Calorim. 2018;3:1835–47.

36. Azizi Z, Alamdari A, Doroodmand MM. Highly stable copper/carbon dot nanofluid. J Therm Anal Calorim. 2018;9:951–60.

37. Zareei M, Yoozbashizadeh H, Reza H, Hosseini M. Investigating the effects of pH, surfactant and ionic strength on the stability of alumina/water nanofluids using DLVO theory. J Therm Anal Calorim. 2018;1:1185–96.

38. Khairul MA, Doroodchi E, Azizian R, Moghtaderi B. Advanced applications of tunable ferrofluids in energy systems and energy harvesters: a critical review. Energ Convers Manage. 2017;149:660–74.

39. Felicia L, Vinod S, Philip J. Recent advances in magnetorheology of critical review. J Nanofluids. 2016;5(1):1–47. https://doi.org/10.1166/jon.2016.1203.

40. Hajiyan M, Ebadi S, Mahmud S, Biglarbegian M. Experimental investigation of the effect of an external magnetic field on the thermal conductivity and viscosity of Fe₃O₄—glycerol International Centre for Diffraction Data. J Therm Anal Calorim. 2018;1:1451–64.

41. Pin Y, Shameli K, Miyake M, Khairudin NBBtA, Mohamad SEBt, Naiki T, Lee KX. Green biosynthesis of superparamagnetic magnetite Fe₃O₄ nanoparticles and biomedical applications in targeted anticancer drug delivery system: a review. Arab J Chem. 2018. https://doi.org/10.1016/j.arabjc.2018.04.013.

42. Brandt JV, Piazza RD, dos Santos CC, Chacón JV, Amantéa BE, Pinto GC, Magnani M, Piva HL, Tedesco AC, Primo FL, Júnior MJ, Marques RFC. Synthesis and colloidal characterization of folic acid-modified PEG-b-PCL Micelles for methotrexate delivery. Colloids Surf B Biointerfaces. 2019;177:228–34.

43. Amantea BE, Piazza RD, Chacon JRV, dos Santos CC, Costa TP, Rocha CO, Brandt JV, Godoi DRM, Júnior MJ, Marques RFC. Esterification influence in thermosensitive behavior of copolymers

PNIPAm- co-PAA and PNVCL-co-PAA in magnetic nanoparticles surface. Colloids Surf A. 2019;575:18–26.

44. De S, Mandal S. Physicochemical and engineering aspects surfactant-assisted shape control of copper nanostructures. Colloids Surf A. 2013;421:72–83.

45. Beriache M, Sidik NAC, Yazid MNAWN, Mamat R, Najafi G, Kefayati GHR. A review on why researchers apply external magnetic field on nanofluids. Int Commun Heat Mass Transf. 2016;78:60–7.

46. Lu A, Salabas EL, Schüth F. Magnetic nanoparticles: synthesis, protection, functionalization, and application. Angewandte. 2007. https://doi.org/10.1002/anie.200602866.

47. Okubo T, Particles E. Fundamentals of Colloid and Surface Chemistry. Colloidal Organization. 2015. https://doi.org/10.1016/b978-0-12-802163-7.00002-7.

48. Bajpai P. Biermann's handbook of pulp and paper: volume 2: paper and board making. Colloid Surf Chem. 2018;19(1):381–400. https://doi.org/10.1016/b978-0-12-814238-7.00019-2.

49. Ohshima H. CHAPTER 1—Interaction of colloidal particles. In: Colloid and interface science in pharmaceutical research and development. Elsevier B.V.; 2014. https://doi.org/10.1016/b978-0-444-62614-1.00001-6.

50. Viali WR, Nunes ES, dos Santos CC, Fermin SWS, Aragón H, Coaquira JAH, Morais PC, Júnior MJ. PEGylation of SPIONs by polycondensation reactions: a new strategy to improve colloidal stability in biological media. J Nanoparticle Res. 2013. https://doi.org/10.1007/s11051-013-1824-x.

51. Abdelbar MF, Fayed TA, Meaz TM, Ebeid E-ZM. Molecular and biomolecular spectroscopy photo-induced interaction of thioglycolic acid (TGA)-capped CdTe quantum dots with cyanine dyes. SAA. 2016;168:1–11.

52. Clayton KN, Salameh JW, Wereley ST, Kinzer-Ursem TL. Physical characterization of nanoparticle size and surface modification using particle scattering diffusometry. Biomicrofluidics. 2016;10:054107.

53. Nakamoto K. Infrared and Raman spectra of inorganic and coordination compounds, part B, applications in coordination, organometallic, and bioinorganic chemistry. 2009.

54. Ferrer EG, Bichara LC, Gramajo B, Brand SA. Vibrational study and force field of the citric acid dimer based on the SQM methodology. Adv Phys Chem. 2011;11:347072-10.

55. Cuadro PD, et al. Reactive, functional polymers cross-linking of cellulose and poly (ethylene glycol) with citric acid. React Funct Polym. 2015;90:21–4.

56. Castillo PM, Mata MDe, Casula MF, Sánchez-alcázar JA, Zaderenko AP. PEGylated versus non-PEGylated magnetic nanoparticles as Camptothecin delivery system. Beilstein J Nanotechnol. 2014;5:1312–9. https://doi.org/10.3762/bjnano.5.144.

57. Tapadiya A, Vasanthan N. Crystallization and alkaline hydrolysis of poly (3-hydroxybutyrate) films probed by thermal analysis and infrared spectroscopy. Int J Biol Macromol. 2017;102:1130–7.

58. Alemdar A, Gungor N, Ece OI, Atici O. The rheological properties and characterization of bentonite dispersions in the presence of non-ionic polymer PEG. J Mater Sci. 2005;40:171–7.

59. Hunter RJ. Foundations of colloid science. 2nd ed. Oxford University Press; 2001.

60. Viali WR, Alcantara GB, Sartoratto PPC, Soler MAG, Mosiniewicz-Szablewska E, Andrzejewski B, Morais PC. Investigation of the molecular surface coating on the stability of insulating magnetic oils. J Phys Chem C. 2010;114(1):179–88.

61. Singh AK. Structure, synthesis, and application of nanoparticles. Eng Nanoparticles. 2016. https://doi.org/10.1016/B978-0-12-801406-6.00002-9.

62. Sun Z, Su F, Forsling W, Samskog P. Surface characteristics of magnetite in aqueous suspension. J Colloid Interface Sci. 1998;159:151–9.

63. Aguilar K, Garvín A, Lara-sagahón AV, Ibarz A. Ascorbic acid degradation in aqueous solution during UV–Vis irradiation. Food Chem. 2019;297:124864.

64. dos Santos CC, Viali WR, Viali ESN, Júnior MJ. Aqueous nanofluids based on thioglycolic acid-coated copper sulfide nanoparticles for heat-exchange applications. J Mol Liq. 2020;313:0167-7322. https://doi.org/10.1016/j.molliq.2020.113391.

65. Hunter RJ. Applications of the Zeta Potential-chapter 6. 1981. https://doi.org/10.1016/b978-0-12-361961-7.50010-9.

66. Shaw DJ. Introduction to colloid and surface chemistry. 1992. https://doi.org/10.1016/C2009-0-24070-0..